Dynamic phase transition, universality, and finite-size scaling in the two-dimensional kinetic Ising model in an oscillating field

G. Korniss,[1,*] C. J. White,[1,2] P. A. Rikvold,[1,2] and M. A. Novotny[1]
[1]*School of Computational Science and Information Technology, Florida State University, Tallahassee, Florida 32306-4120*
[2]*Center for Materials Research and Technology and Department of Physics, Florida State University, Tallahassee, Florida 32306-4350*

(Received 8 August 2000; published 27 December 2000)

We study the two-dimensional kinetic Ising model below its equilibrium critical temperature, subject to a square-wave oscillating external field. We focus on the multidroplet regime, where the metastable phase decays through nucleation and growth of *many* droplets of the stable phase. At a critical frequency, the system undergoes a genuine nonequilibrium phase transition, in which the symmetry-broken phase corresponds to an asymmetric stationary limit cycle for the time-dependent magnetization. We investigate the universal aspects of this dynamic phase transition at various temperatures and field amplitudes via large-scale Monte Carlo simulations, employing finite-size scaling techniques adopted from equilibrium critical phenomena. The critical exponents, the fixed-point value of the fourth-order cumulant, and the critical order-parameter distribution all are consistent with the universality class of the two-dimensional *equilibrium* Ising model. We also study the cross-over from the multidroplet regime to the strong-field regime, where the transition disappears.

DOI: 10.1103/PhysRevE.63.016120 PACS number(s): 64.60.Ht, 75.10.Hk, 64.60.Qb, 05.40.−a

I. INTRODUCTION

Metastability and hysteresis are widespread phenomena in nature. Ferromagnets are common systems that exhibit these behaviors [1–5], but there are also numerous other examples ranging from ferroelectrics [6,7] to electrochemical adsorbate layers [8,9] to liquid crystals [10]. A simple model for many of these real systems is the kinetic Ising model (in either the spin- or lattice-gas representation). For example, it was shown to be appropriate for describing magnetization dynamics in highly anisotropic single-domain nanoparticles and uniaxial thin films [11–14].

The system response to a single reversal of the ''external field'' is fairly well understood [15]. In sufficiently large systems below the equilibrium critical temperature T_c, the order parameter changes its value through the nucleation and growth of *many* droplets, inside which it has an equilibrium value consistent with the value of the applied field, as shown in Fig. 1. This is the multidroplet regime of phase transformation [15,16]. The well-known Avrami's law [17] describes this process of homogeneous nucleation followed by growth quite accurately up to the time when the growing droplets coalesce and the stable phase becomes the majority phase [18]. The intrinsic time scale of the system is given by the metastable lifetime $\langle \tau \rangle$, which is defined as the average first-passage time to zero magnetization. This is a measure of the time it takes for the system to escape from the metastable region of the free-energy landscape. In this paper we will use the magnetic language in which the order parameter is the magnetization m, and its conjugate field is the external magnetic field H. Analogous interpretations, e.g., using the terms ''polarization'' and ''electric field'' for ferroelectric systems [6,7], and ''coverage'' and ''chemical potential'' for adsorption problems [8,9], are straightforward.

It is natural next to ask, ''what is the response to an oscillating external field?'' The hysteretic behavior in ferromagnets has attracted significant experimental interest, mainly focused on the characteristic behavior of the hysteresis loop and its area. Its dependence on the field amplitude and frequency was intensively studied, and its scaling behavior (power law versus logarithmic) is still under investigation, both experimentally [11–13] and theoretically [19–27]. For a kinetic Ising ferromagnet in two dimensions it was recently shown [25–27] that the true behavior is in fact a crossover, approaching a logarithmic frequency dependence only for extremely low frequencies.

An important aspect of hysteresis in bistable systems, which is the focus of the present paper, is the dynamic competition between the two time scales in the system: the half-period of the external field $t_{1/2}$ (proportional to the inverse of

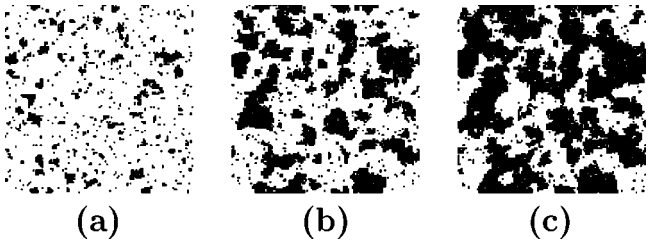

FIG. 1. Metastable decay in the multidroplet regime at $T=0.8T_c$ for an $L=128$ square-lattice kinetic Ising system evolving under Glauber dynamics. The system is initialized with all spins $s_i=1$, and an applied field $H=-0.3J$ is set at $t=0$. Snapshots of the spin configurations are given at (a) $t=30$ Monte Carlo steps per spin (MCSS), (b) $t=60$ MCSS, and (c) $t=74$ MCSS. The metastable lifetime (the average first-passage time to zero magnetization) at this temperature and field is $\langle \tau \rangle = 74.5$ MCSS. Stable $s=-1$ (metastable $s=+1$) spins are represented by black (white).

*Permanent address: Department of Physics, Applied Physics, and Astronomy, Rensselaer Polytechnic Institute, Troy, NY 12180-3590.

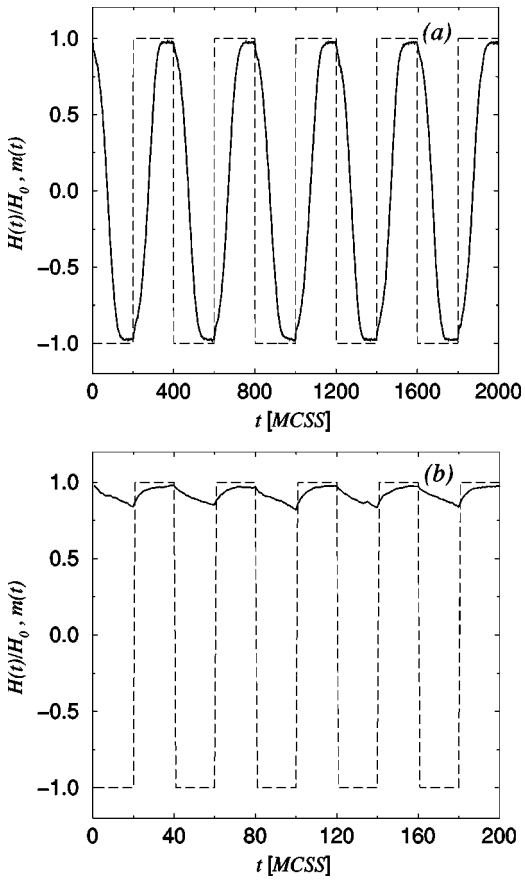

FIG. 2. Monte Carlo magnetization time series (solid lines) in the presence of a square-wave external field (dashed lines) for an $L=128$ system at $T=0.8T_c$ and field amplitude $H_0=0.3J$. (T_c is the two-dimensional equilibrium Ising critical temperature.) The metastable lifetime at this temperature and field is $\langle\tau\rangle=74.5$ MCSS. (a) Dynamically disordered phase at dimensionless half-period $\Theta\equiv t_{1/2}/\langle\tau\rangle=2.7$. (b) Dynamically ordered phase at $\Theta=0.27$.

the driving frequency), and the metastable lifetime $\langle\tau\rangle$. For low frequencies, a complete decay of the metastable phase almost always occurs in each half-period, just as it does after a single field reversal. Consequently, the time-dependent magnetization reaches a limit cycle which is symmetric about zero [Fig. 2(a)]. For high frequencies, however, the system does not have enough time to switch during one half-period, and the symmetry of the hysteresis loop is broken. The magnetization then reaches an asymmetric limit cycle [Fig. 2(b)]. Avrami's law [17,18] is a good approximation when the majority of the droplets do not overlap. Thus it can be employed to estimate the time-dependent magnetization and the dynamic order parameter (period-averaged magnetization) in the low-frequency (see the Appendix) and high-frequency [27] limits. However, it cannot describe the ''critical regime'' where $t_{1/2}$ becomes comparable to $\langle\tau\rangle$, and which is dominated by coalescing droplets.

This symmetry breaking between the symmetric and asymmetric limit cycles has been the subject of intensive research over the last decade. It was first observed during numerical integration of a mean-field equation of motion for the magnetization of a ferromagnet in an oscillating field [21,22]. Since then, it was observed and studied in numerous Monte Carlo (MC) simulations of kinetic Ising systems [24,27–33], as well as in further mean-field studies [23,29,31,32,34]. It may also have been experimentally observed in ultrathin films of Co on Cu(001) [12]. The results of these studies suggest that this symmetry breaking corresponds to a genuine continuous nonequilibrium phase transition. For recent reviews, see Refs. [35,36]. Associated with the transition is a divergent time scale (critical slowing down) [31] and, for spatially extended systems, a divergent correlation length [27,28]. Estimates for the critical exponents and the universality class of the transition recently became available [27,28,37] after the successful application of finite-size scaling techniques borrowed from equilibrium critical phenomena [38–41].

The purpose of the present paper is to extend preliminary results [37], and to provide more accurate estimates of the exponents for two-dimensional kinetic Ising systems in a square-wave oscillating field. The use of the square-wave field tests the universality of the dynamic phase transition (DPT) [27,28], and it also significantly increases computational speed, compared to the more commonly used sinusoidal field. We further explore the universal aspects of the transition by varying the temperature and field amplitude within the multidroplet regime, and we study the crossover to the strong-field regime where the transition disappears. In obtaining our results, we rely on dynamic MC simulations. Computational methods are always helpful, especially when theoretical ideas are largely missing. There are cases, however, when even the use of standard equilibrium techniques, such as finite-size scaling, requires some insight and building of analogies between equilibrium and nonequilibrium systems [27,28]. This is the case for our present study. To our knowledge, no effective ''Hamiltonian'' was known before the completion of this work for the dynamic order parameter (in the coarse-grained sense), from which the long-distance behavior of the model could be derived. This is a typical difficulty when dealing with systems far from equilibrium [42,43]. Recently, however, a coarse-grained Hamiltonian was derived [44] for the dynamic order parameter, supporting our results for the DPT. Similar to the previous work for sinusoidally oscillating fields [27,28], we perform large-scale simulations and finite-size scaling to investigate the universal properties of the DPT.

The remainder of the paper is organized as follows. In Sec. II we define the model and the observables of interest. Section III contains the Monte Carlo results and analyses. Conclusions and an outlook are given in Sec. IV.

II. MODEL AND RELEVANT OBSERVABLES

To model spatially extended bistable systems in two dimensions, we study a nearest-neighbor kinetic Ising ferromagnet on an $L\times L$ square lattice with periodic boundary conditions. The model is defined by the Hamiltonian

$$\mathcal{H}=-J\sum_{\langle ij\rangle}s_is_j-H(t)\sum_i s_i\,, \tag{1}$$

where $s_i = \pm 1$ is the state of the ith spin, $J>0$ is the ferromagnetic interaction, $\Sigma\langle ij\rangle$ runs over all nearest-neighbor pairs, Σ_i runs over all L^2 lattice sites, and $H(t)$ is an oscillating, spatially uniform applied field. The magnetization per site,

$$m(t) = \frac{1}{L^2}\sum_{i=1}^{L^2} s_i(t), \tag{2}$$

is the density conjugate to $H(t)$. The temperature T is fixed below its zero-field critical value T_c [$J/k_B T_c = \ln(1+\sqrt{2})/2$ [45], where k_B is Boltzmann's constant], so that the magnetization for $H=0$ has two degenerate spontaneous equilibrium values, $\pm m_{sp}(T)$. For nonzero fields the equilibrium magnetization has the same sign as H, while for H not too strong, the opposite magnetization direction is *metastable* and decays slowly towards equilibrium with time, as described in Sec. I.

The dynamic used in this study, as well as in Refs. [27,28], is the Glauber single-spin-flip MC algorithm with updates at randomly chosen sites. Note that the random sequential update scheme corresponds to independent Poisson arrivals for the update attempts (discrete events) at each site. Thus the arrival pattern is strongly asynchronous. The time unit is one MC step per spin (MCSS). Each attempted spin flip from s_i to $-s_i$ is accepted with probability

$$W(s_i \to -s_i) = \frac{\exp(-\beta\Delta E_i)}{1+\exp(-\beta\Delta E_i)}. \tag{3}$$

Here ΔE_i is the energy change resulting from acceptance, and $\beta = 1/k_B T$. For the largest system studied ($L=512$) we used a scalable massively parallel implementation of the algorithm for this *asynchronous* dynamics [46–49]. The parallel discrete-event scheme ensures that the underlying dynamic is not changed (that is, the update attempts are identical, independent Poisson arrivals at each site), while a substantial amount of parallelism is exploited. The parallel implementation [47] was carried out on a Cray T3E, employing up to 256 processing elements.

The dynamic order parameter is the period-averaged magnetization [21]

$$Q = \frac{1}{2t_{1/2}}\oint m(t)dt, \tag{4}$$

where $t_{1/2}$ is the half-period of the oscillating field, and the beginning of the period is chosen at a time when $H(t)$ changes sign. Although the phase of the field does not influence the results reported in this paper, the choice made here is convenient in studies of the hysteresis loop-area distributions and consistent with Refs. [25–28]. Analogously we also define the local order parameter

$$Q_i = \frac{1}{2t_{1/2}}\oint s_i(t)dt, \tag{5}$$

which is the period-averaged spin at site i. For slowly varying fields the probability distribution of Q is sharply peaked at zero [27,28]. We shall refer to this as the *dynamically disordered phase*. It is illustrated by the evolution of the magnetization in Fig. 2(a) and by the $Q \approx 0$ time series in Fig. 3. For rapidly oscillating fields the distribution of Q becomes bimodal with two sharp peaks near $\pm m_{sp}(T)$, corresponding to the broken symmetry of the hysteresis loops [27,28]. We shall refer to this as the *dynamically ordered phase*. It is illustrated in Fig. 2(b) and by the $Q \approx m_{sp} \sim O(1)$ time series in Fig. 3. Near the DPT we use finite-size scaling analysis of MC data to estimate the critical exponents that characterize the transition. We also keep track of the normalized period-averaged internal energy (in units of J) [31],

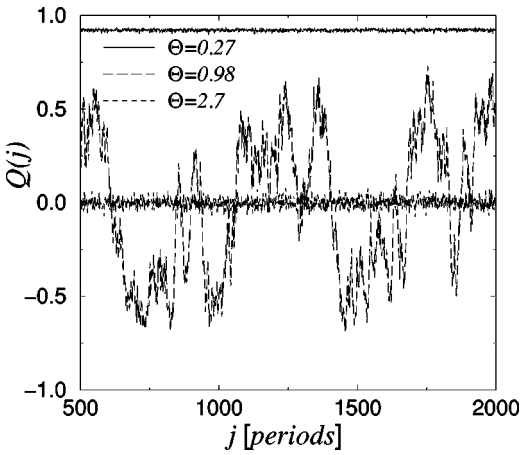

FIG. 3. Time series of the order parameter Q at $T=0.8T_c$ and $H_0=0.3J$ for $L=128$. Horizontal trace near $Q=+1$: $\Theta=0.27 < \Theta_c$ [dynamically ordered phase, corresponding to Fig. 2(b)]. Strongly fluctuating trace: $\Theta=0.98 \approx \Theta_c$ (near the DPT). Horizontal trace near $Q=0$: $\Theta=2.7 > \Theta_c$ [dynamically disordered phase, corresponding to Fig. 2(a)].

$$E = -\frac{1}{2t_{1/2}}\oint \frac{1}{L^2}\sum_{\langle ij\rangle} s_i(t)s_j(t)dt, \tag{6}$$

since it also exhibits important characteristics of the DPT.

Previous studies of the DPT used an applied field which varies sinusoidally in time. While sinusoidal or linear sawtooth fields are the most common in experiments, and are necessary to obtain a vanishing loop area in the low-frequency limit [25–27], the wave form of the field should not affect universal aspects of the DPT. This should be so because the transition essentially depends on the competition between two time scales: the half-period $t_{1/2}$ of the applied field, and the average time it takes the system to leave the metastable region near one of its two degenerate zero-field equilibria when a field of magnitude H_0 and sign opposite to the magnetization is applied. This *metastable lifetime*, $\langle \tau(T,H_0)\rangle$, is estimated as the average first-passage time to zero magnetization. In the present paper we use a *square-wave* field of amplitude H_0. This has significant computational advantages over the sinusoidal field variation, since we can use two look-up tables to determine the acceptance probabilities: one for $H=+H_0$ and one for $H=-H_0$.

In terms of the dimensionless half-period,

$$\Theta = t_{1/2}/\langle \tau(T,H_0)\rangle, \tag{7}$$

the DPT should occur at a critical value Θ_c of order unity. Although Θ can be changed by varying either $t_{1/2}$, H_0, or T, in a first approximation we expect Θ_c to depend only weakly on H_0 and T. This expectation will be confirmed in Sec. IV by simulations carried out at several values of H_0 and T for different system sizes.

In many studies of the DPT the transition has been approached by changing H_0 or T [24,29,30,32]. While this is correct in principle, $\langle \tau(T,H_0)\rangle$ depends strongly and nonlinearly on its arguments [15]. We therefore prefer changing $t_{1/2}$ at constant H_0 and T [27,28], as this gives more precise control over the distance from the transition.

We focus on systems which are not only larger than the critical droplet, but also significantly larger than the typical droplet separation [15]. In this regime *many* supercritical droplets form and contribute to the decay of the metastable phase the Kolmogorov–Johnson-Mehl–Avrami (KJMA) or Avrami theory for homogeneous nucleation [17,18]), as seen in Fig. 1. This is the only regime where the DPT is expected to exist. For small systems one observes subtle finite-size effects, not related to the DPT but rather to the *stochastic* single-droplet decay mode [15,50]. In the single-droplet regime, subject to a periodic applied field, the system exhibits stochastic resonance [26].

III. SIMULATION RESULTS

A. Signs of the dynamic phase transition

We performed extensive simulations and finite-size scaling analysis of the data on square lattices with L between 64 and 512 at $T=0.8T_c$ and $H_0=0.3J$. We also investigated the universality of the DPT within the multidroplet regime for various fields and temperatures below the equilibrium critical temperature, using smaller systems with L from 64 to 128. Typical runs near the DPT consist of 2×10^5 full periods. For example, at $T=0.8T_c$ and $H_0=0.3J$, where the critical half-period of the field is about 70 MCSS, this corresponds to 2.8×10^7 MCSS. Away from the transition point, an order of magnitude shorter runs were sufficient to obtain high-quality statistics.

The system was initialized with all spins up, and the square-wave external field started with a half-period in which $H=-H_0$. After some relaxation the system magnetization would reach a limit cycle (Fig. 2) (except for thermal fluctuations). In other words, Q [Eq. (4)] (together with other period-averaged quantities) becomes a *stationary* stochastic process (Fig. 3). We discarded the first 1000 periods of the time series to exclude transients from the stationary-state averages.

For large half-periods ($\Theta \gg \Theta_c$) the magnetization switches every half-period [Fig. 2(a)] and $Q\approx 0$, while for small half-periods ($\Theta \ll \Theta_c$) the magnetization does not have time to switch during a single half-period [Fig. 2(b)], resulting in $|Q|\approx m_{\rm sp}$, as can be seen from the time series in Fig. 3. The transition between the high- and low-frequency regimes is characterized by large fluctuations in Q near Θ_c (Fig. 3).

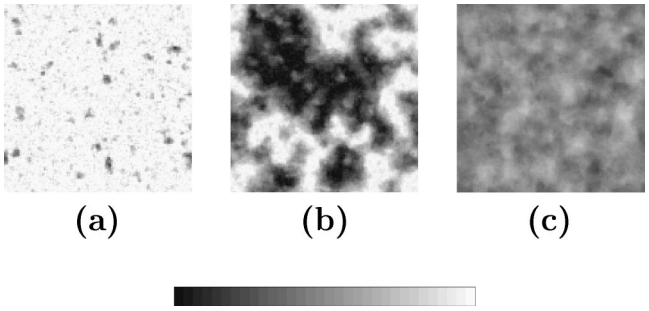

FIG. 4. Configurations of the local order parameter $\{Q_i\}$ at $T=0.8T_c$ and $H_0=0.3J$ for $L=128$. The ''snapshots'' of $\{Q_i\}$ for each regime are the set of local period-averaged spins during some representative period. (a) $\Theta=0.27<\Theta_c$ (dynamically ordered phase). (b) $\Theta=0.98\approx\Theta_c$ (near the DPT). (c) $\Theta=2.7>\Theta_c$ (dynamically disordered phase). On the gray scale black (white) corresponds to -1 $(+1)$.

To illustrate the spatial aspects of the transition, we also show configurations of the local order parameter $\{Q_i\}$ in Fig. 4. Below Θ_c [Fig. 4(a)] the majority of spins spend most of their time in the $+1$ state, i.e., in the metastable phase during the first half-period, and in the stable equilibrium phase during the second half-period (except for equilibrium fluctuations). Thus most of the $Q_i\approx+1$. Droplets of $s_i=-1$ that nucleate during the negative half-period and then decay back to $+1$ during the positive half-period show up as roughly circular gray spots in the figure. Since the spins near the center of such a droplet become negative first and revert to positive last, these spots appear darkest in the middle. Also, for not too large lattices, one occasionally observes a full reversal of an ordered configuration $\{Q_i\}\rightarrow\{-Q_i\}$, typical of finite, spatially extended systems undergoing symmetry breaking. Above Θ_c [Fig. 4(c)], the system follows the field in every half-period (with some phase lag) and $Q_i\approx0$ at all sites i. Near Θ_c [Fig. 4(b)] there are large clusters of both $Q_i\approx+1$ and $Q_i\approx-1$ separated by ''interfaces'' where $Q_i\approx0$. These large-scale structures remain reasonably stationary over several periods.

For finite systems in the dynamically ordered phase the probability density of Q becomes bimodal. Thus, to capture symmetry breaking, one has to measure the average norm of Q as the order parameter, i.e., $\langle|Q|\rangle$ [39]. Figure 5(a) shows that this order parameter is of order unity for $\Theta<\Theta_c$, and vanishes for $\Theta>\Theta_c$, except for finite-size effects. To characterize and quantify this transition in terms of critical exponents, we employ the well-known technique of finite-size scaling [38–41]: The quantity analogous to the susceptibility is the scaled variance of the dynamic order parameter [27,28]:

$$X_L^Q = L^2(\langle Q^2\rangle_L - \langle|Q|\rangle_L^2). \tag{8}$$

Note that for our system the field conjugate to Q and a corresponding fluctuation-dissipation theorem are not known; hence we cannot measure the susceptibility directly. For finite systems X_L has a characteristic peak near Θ_c [see Fig.

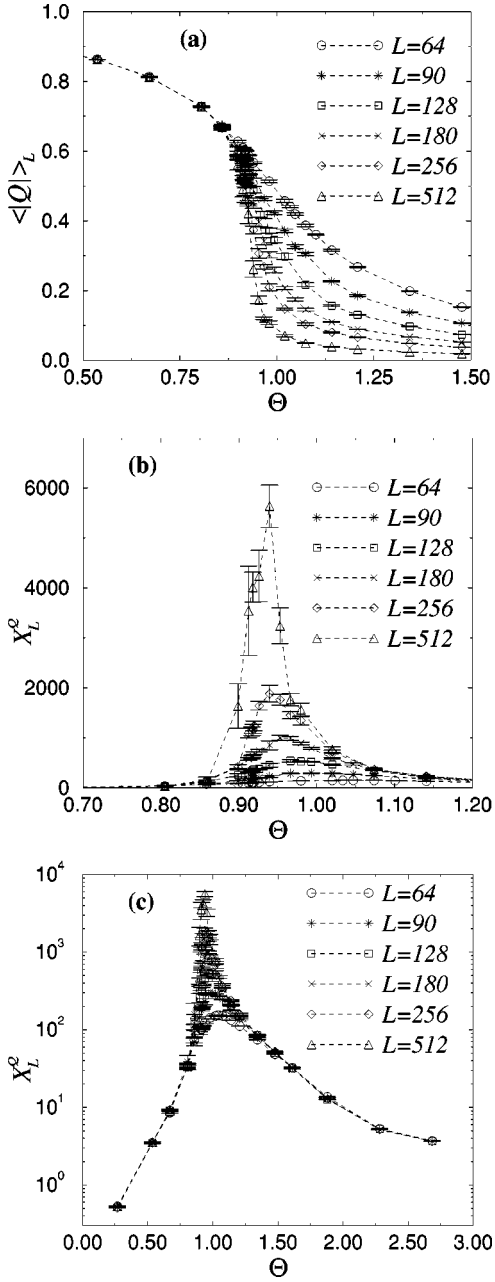

FIG. 5. Finite-size behavior of the order parameter at $T=0.8T_c$ and $H_0=0.3J$ for various system sizes. (a) The order parameter $\langle|Q|\rangle_L$. (b) The scaled variance of the order parameter, X_L^Q, as defined in Eq. (8). (c) Same as in (b) on a lin-log scale to provide an enhanced view of the peaks for smaller systems.

5(b)] which increases in height with increasing L, while no finite-size effects can be observed for $\Theta \ll \Theta_c$ and $\Theta \gg \Theta_c$. This implies the existence of a divergent length scale, possibly the correlation length which governs the long-distance behavior of the local order-parameter correlations $\langle Q_i Q_j \rangle$. The location of the maximum in X_L^Q also shifts with L, which gives further important information about the critical exponents.

The normalized stationary time-displaced autocorrelation function of the order parameter,

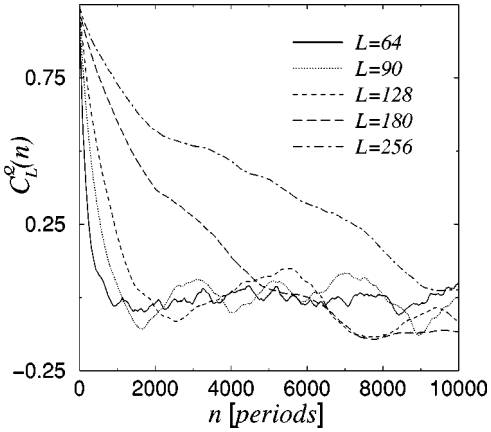

FIG. 6. Critical slowing down for the order parameter at $T=0.8T_c$ and $H_0=0.3J$ at $\Theta=\Theta_c$, as shown by the normalized autocorrelation function $C_L^Q(n)$.

$$C_L^Q(n)=\frac{\langle Q(j)Q(j+n)\rangle-\langle Q(j)\rangle^2}{\langle Q^2(j)\rangle-\langle Q(j)\rangle^2}, \tag{9}$$

provides further insights into the DPT as the system exhibits critical slowing down (Fig. 6). This can be seen as increasing correlation times with increasing system sizes. In Sec. III D we provide a quantitative analysis of the correlation times.

We also measured the period-averaged internal energy [Eq. (6)] and its fluctuations [31],

$$X_L^E=L^2(\langle E^2\rangle_L-\langle E\rangle_L^2), \tag{10}$$

as can be seen in Fig. 7. The peaks of these fluctuations exhibit a slow increase with the system size (compared to the order-parameter fluctuations), as one may anticipate by analogy with the equilibrium heat capacity.

B. Finite-size scaling

Scaling laws and finite-size scaling for equilibrium systems with an *a priori* known Hamiltonian can be systematically derived using the concepts of the free energy and the renormalization group [51]. The kinetic Ising model with the explicitly time-dependent Hamiltonian Eq. (1) is driven far from equilibrium. Although the order-parameter distribution $P(Q)$ is stationary, the effective Hamiltonian controlling its fixed-point behavior was not known until recently [44] (after the completion of this study). Motivated by the similarity of the finite-size effects shown in Figs. 5–7 to those characteristic of a typical continuous phase transition, we borrow the corresponding scaling assumptions from equilibrium finite-size scaling. For our model the quantity analogous to the reduced temperature in equilibrium systems (i.e., the distance from the *infinite*-system critical point) is

$$\theta=\frac{|\Theta-\Theta_c|}{\Theta_c}. \tag{11}$$

Finite-size scaling theory provides simple scaling relations for the observables for finite systems in the critical regime [39,40],

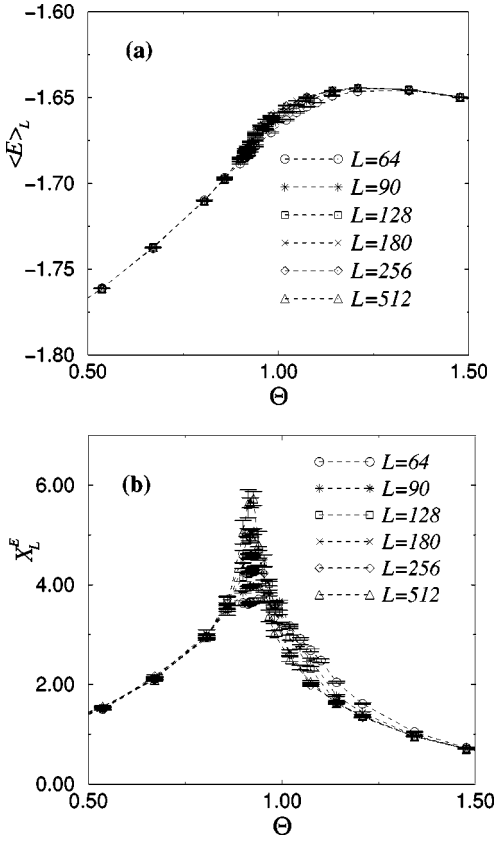

FIG. 7. Finite-size behavior of the period-averaged internal energy at $T=0.8T_c$ and $H_0=0.3J$ for various system sizes. (a) The period-averaged internal energy. (b) The scaled energy variance X_L^E as defined in Eq. (10).

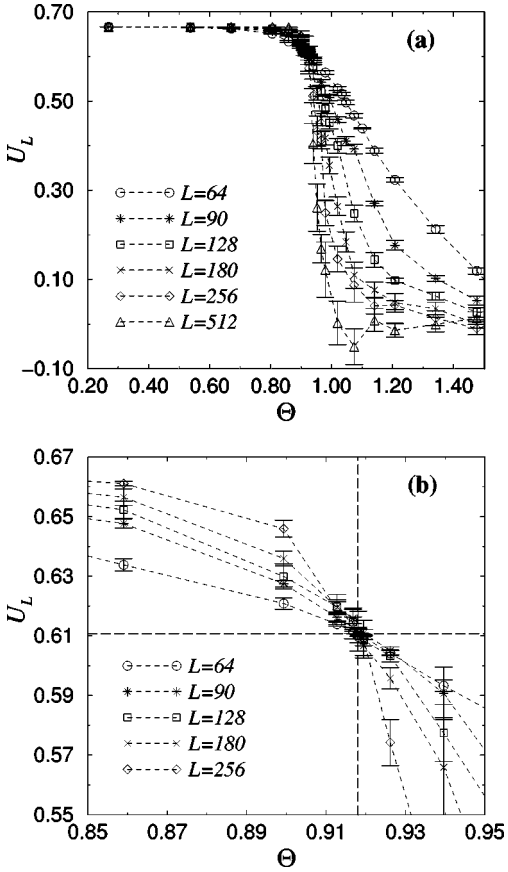

FIG. 8. (a) The fourth-order cumulant as defined in Eq. (15) at $T=0.8T_c$ and $H_0=0.3J$ for various system sizes. (b) The region around the cumulant crossing in (a) enlarged. The horizontal and vertical dashed lines indicate the fixed-point value $U^*=0.611$ and the scaled critical half-period $\Theta_c=0.918$, respectively.

$$\langle |Q| \rangle_L = L^{-\beta/\nu} \mathcal{F}_{\pm}(\theta L^{1/\nu}), \tag{12}$$

$$X_L^Q = L^{\gamma/\nu} \mathcal{G}_{\pm}(\theta L^{1/\nu}), \tag{13}$$

$$X_L^E = c_1 \ln[L \mathcal{J}_{\pm}(\theta L^{1/\nu})], \tag{14}$$

where $\mathcal{F}_{\pm}$, $\mathcal{G}_{\pm}$, and $\mathcal{J}_{\pm}$ are scaling functions, and the $+$ $(-)$ index refers to $\Theta > \Theta_c$ $(\Theta < \Theta_c)$. The logarithmic scaling in X_L^E is motivated by the very slow divergence of the scaled period-averaged energy variance [Fig. 7(b)]. The above formulation of scaling is explicitly based on the infinite-system critical point Θ_c, which can be estimated with far greater accuracy than the location of the maximum of the order-parameter fluctuations for the individual finite system sizes. We use the fourth-order cumulant intersection method [39,40] to estimate the value of Θ_c at which the transition occurs in an *infinite* system. In order to do this, we plot

$$U_L = 1 - \frac{\langle Q^4 \rangle_L}{3\langle Q^2 \rangle_L^2} \tag{15}$$

as a function of Θ for several system sizes, as shown in Fig. 8. For the largest system ($L=512$) the statistical uncertainty in U_L was too large to use it to obtain estimates for the crossing. Our estimate for the dimensionless critical half-period, based on the remaining five system sizes, is $\Theta_c = 0.918 \pm 0.005$, with a fixed-point value $U^* = 0.611 \pm 0.003$ for the cumulant [Fig 8(b)].

Then, at Θ_c, the scaling forms [Eqs. (12–14)] yield

$$\langle |Q| \rangle_L \propto L^{-\beta/\nu}, \tag{16}$$

$$X_L^Q \propto L^{\gamma/\nu}, \tag{17}$$

$$X_L^E \propto c_2 + c_1 \ln(L), \tag{18}$$

which enable us to estimate the exponent ratios β/ν and γ/ν, and to directly check the postulated logarithmic divergence in the period-averaged energy fluctuations. Plotting $\langle |Q| \rangle_L$ and X_L^Q at Θ_c, and utilizing a weighted linear least-squares fit to the logarithmic data, yields $\beta/\nu = 0.126 \pm 0.005$ [Fig. 9(a)] and $\gamma/\nu = 1.74 \pm 0.05$ [Fig. 9(b)]. Note that these values are extremely close (within statistical errors) to the corresponding ratios for the *equilibrium* two-dimensional Ising universality class, $\beta/\nu = 1/8 = 0.125$ and $\gamma/\nu = 7/4 = 1.75$. Further, the straight line in Fig. 9(c) indicates the slow logarithmic divergence of X_L^E at the critical point. In addition to the scaling at Θ_c, we also checked the divergences of the peaks of the fluctuations, $(X_L^Q)_{\text{peak}}$ and $(X_L^E)_{\text{peak}}$, since they

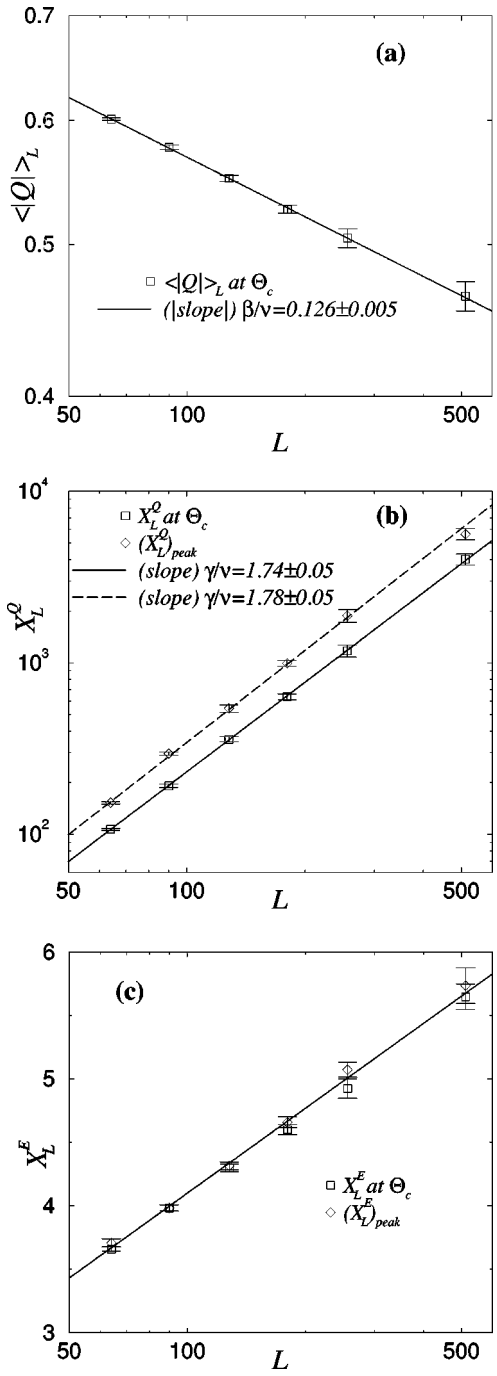

FIG. 9. Critical exponent estimates at $T=0.8T_c$ and $H_0=0.3J$. Straight lines are the weighted least-square fits. (a) Determining β/ν through the finite-size effects of the order parameter, based on Eq. (16) (log-log plot). (b) Determining γ/ν through the finite-size effects of the order-parameter fluctuations, based on Eq. (17) (log-log plot). (c) Showing the logarithmic divergence of the period-averaged energy fluctuations, based on Eq. (18) (log-lin plot).

asymptotically should follow the same scaling laws, Eqs. (17) and (18), respectively. The measured exponent $\gamma/\nu = 1.78 \pm 0.05$ for $(X_L^Q)_{\text{peak}}$ and the logarithmic divergence for $(X_L^E)_{\text{peak}}$ agree to within the statistical errors with the results obtained at Θ_c, as can be seen in Figs. 9(b) and 9(c), respectively.

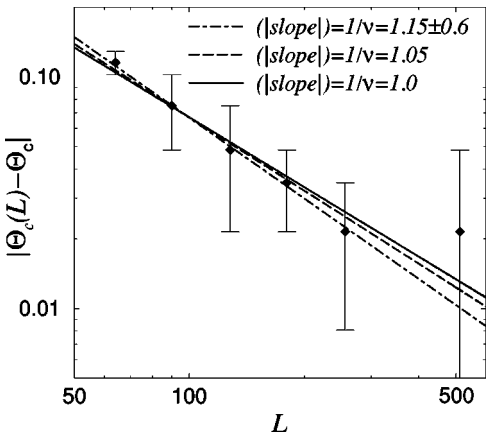

FIG. 10. Exponent estimate for ν at $T=0.8T_c$ and $H_0=0.3J$, based on Eq. (19) (log-log plot). The dot-dashed line is a weighted least-squares fit (excluding the smallest and the largest system), yielding the slope $1/\nu=1.15\pm0.6$ ($\nu=0.87\pm0.4$). The dashed line represents the ''optimal'' value for this exponent, using the best quality data collapse for the scaling function [Eq. (12)] as discussed in the text, yielding $1/\nu=1.05$ ($\nu=0.95$). The solid line represents the two-dimensional equilibrium Ising exponent $\nu=1.0$.

From the finite-system shifting of the transition one can estimate the correlation-length exponent ν by tracking the shift in the location of the maximum in X_L^Q,

$$|\Theta_c(L)-\Theta_c| \propto L^{-1/\nu}, \tag{19}$$

where $\Theta_c(L)$ is the location of the peak for finite systems. However, the precision of this method for our data is very poor, due to limited resolution in finding the locations of the maxima and consequently the large relative errors in $|\Theta_c(L)-\Theta_c|$. Excluding the smallest (due to strong corrections to scaling) and largest systems (due to very poor resolution and extremely large statistical error), we obtain $\nu = 0.87 \pm 0.4$, but the large error estimate obviously implies a rather poor accuracy (Fig. 10).

To obtain a more complete picture of how well the scaling relations in Eqs. (12) and (13) hold, we plot $\langle|Q|\rangle_L L^{\beta/\nu}$ [Fig. 11(a)] and $X_L^Q L^{-\gamma/\nu}$ [Fig. 11(b)] vs $\theta L^{1/\nu}$ [41]. For the exponent ratios we used $\beta/\nu=1/8=0.125$ and $\gamma/\nu=7/4 = 1.75$, since our estimate for those (within small statistical errors) implied that they take on the equilibrium two-dimensional Ising universal values. Most importantly, we used various values of ν between 0.5 and 1.2 to find the best data collapse as observed visually, since our estimate for this exponent was far from reliable. The ''optimal'' value obtained this way (by showing scaling plots to group members who did not know the particular values of ν used), and used in Figs. 11(a) and 11(b), is $\nu=0.95\pm0.15$. Full scaling plots using the exact Ising exponents are also shown in Figs. 11(c) and 11(d), and they result in similarly good data collapse.

C. Order-parameter histograms at criticality

We devote this subsection to analyzing the universal characteristics of the full order-parameter distribution $P(Q)$ at the critical point. This distribution is bimodal for finite sys-

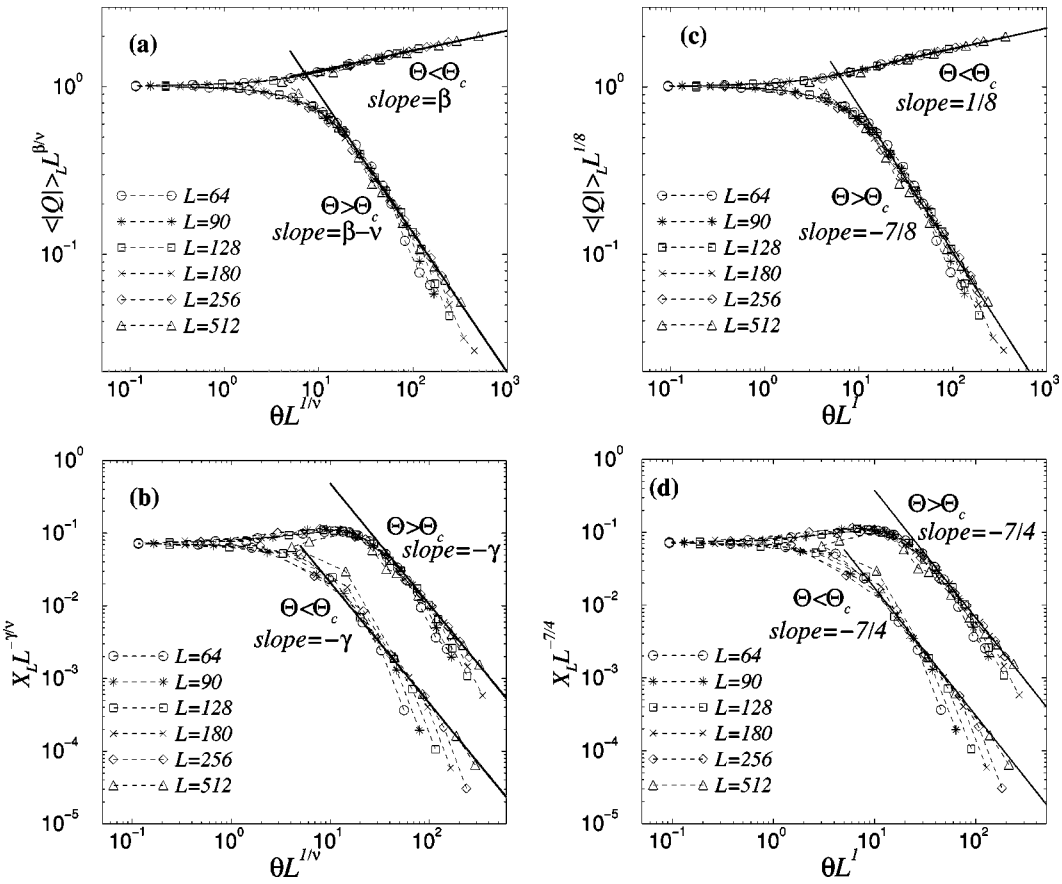

FIG. 11. Finite-size scaling (full data collapse) at $T=0.8T_c$ and $H_0=0.3J$ using $\beta/\nu=1/8$, $\gamma/\nu=7/4$ (two-dimensional equilibrium Ising values), and $\nu=0.95$ (which yields the best quality data collapse). (a) For the order parameter $\langle|Q|\rangle_L$ (log-log plot). (b) For the scaled order-parameter variance X_L^Q (log-log plot). Straight lines in both graphs represent the asymptotic large-argument behaviors of the scaling functions $\mathcal{F}_\pm$ and $\mathcal{G}_\pm$ given in Eqs. (12) and (13), respectively. (c) and (d) are the same as (a) and (b), except that the exact Ising exponent $\nu=1.0$ is used.

tems if observed for sufficiently long times (Fig. 12) [52]. It is more convenient to focus on the distribution of $|Q|$, avoiding the effect of the insufficient number of switching events between the two symmetry-broken phases for large systems, which causes the skewness in Fig. 12(b). Figure 13(a) shows the order-parameter distributions $P_L(|Q|)$ at the critical point for various system sizes. Finite-size scaling arguments [39,40] suggest that, at Θ_c,

$$P_L(|Q|)=L^{\beta/\nu}\mathcal{P}(L^{\beta/\nu}|Q|). \tag{20}$$

Thus the scaled distributions $L^{-\beta/\nu}P_L(|Q|)$ vs $x=|Q|L^{\beta/\nu}$ should fall on the same curve $\mathcal{P}(x)$ for different system sizes. Again, we used $\beta/\nu=1/8$. The quality of the data collapse is quite impressive [Fig. 13(b)], with deviations mainly observed for the smallest L and the largest values of $|Q|$ [Fig. 13(c)], possibly as a result of corrections to scaling.

What we find somewhat surprising, is that the distribution appears to be identical (except for stronger corrections to scaling for the DPT) to that of the equilibrium two-dimensional Ising model on a square lattice with periodic boundary conditions at criticality, *without* a need for any additional scaling parameters. We checked this by performing standard equilibrium two-dimensional Ising simulations with Glauber dynamics and system sizes ranging from $L=64$ to 128, and also by comparing our scaled DPT order-parameter histograms to the high-precision two-dimensional equilibrium Ising MC data of Ref. [53] (Fig. 13). We had expected the *shapes* of the distributions to be identical for the DPT and the equilibrium Ising model, as a consequence of the identical values for the cumulant fixed-point value U^*. However, it is not obvious to us why the microscopic length scales in the DPT and the equilibrium Ising model also appear to be identical, as evidenced by the absence of the need for an additional scaling $L\to L/a$ (a being the microscopic length scale in the DPT).

D. Critical slowing down

Computing the stationary autocorrelation function given by Eq. (9), we already pointed out that at Θ_c the correlation time increases quickly with system size (Fig. 6). Correlation times are typically extracted from an exponential decay as

$$C_L^Q(n)\propto e^{-n/\tau_L^Q}, \tag{21}$$

and they are expected to be finite for finite systems. The

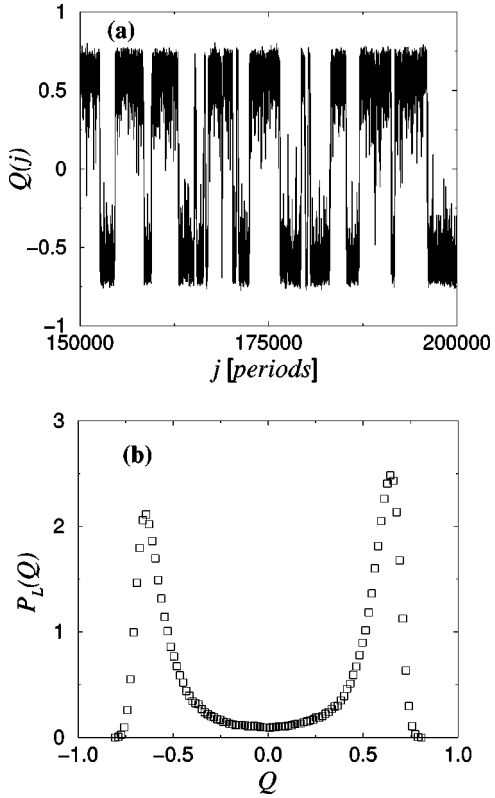

FIG. 12. (a) Short segment of the order-parameter time series at $T=0.8T_c$ and $H_0=0.3J$ for an $L=128$ system at Θ_c [52]. (b) Order-parameter histogram for the same parameters.

correlation time τ_L^Q is also well defined in the $L\to\infty$ limit *away* from the transition. However, it diverges with L at the transition point as

$$\tau_L^Q \propto L^z, \tag{22}$$

where z is the dynamical critical exponent. For correlations measured at intermediate time intervals, we had reasonable statistics including the larger systems (up to $L=256$) to fit the usual exponential decay [Fig. 14(a)]. Then, plotting the correlation times τ_L^Q vs L yields the dynamic exponent $z=1.91\pm0.15$, as shown in Fig. 14(b). Note that from the local Glauber dynamic for the spins there does not directly follow any dynamic which governs the evolution of $\{Q_i\}$. In this respect, it is somewhat surprising that our value for z at the DPT is within two standard deviations of most estimates for the dynamic exponent of the two-dimensional equilibrium Ising model with local dynamics [54].

E. Universality for various temperatures and fields and crossover to the strong-field regime

The underlying ingredient for the spatially extended bistable systems exhibiting a DPT is the local metastability (and the corresponding characteristic time spent in the metastable ''free-energy well'') in the presence of an external field. This, in turn, provides a competition between time scales if the system is driven by a periodic field. Based on this, we expect that sufficiently large systems (in which many droplets contribute to the decay of the metastable phase) exhibit a DPT at a half-period $t_{1/2}$ comparable to the metastable lifetime $\langle\tau(T,H_0)\rangle$. In other words, we expect the critical dimensionless half-period to be of order 1, $\Theta_c \sim O(1)$.

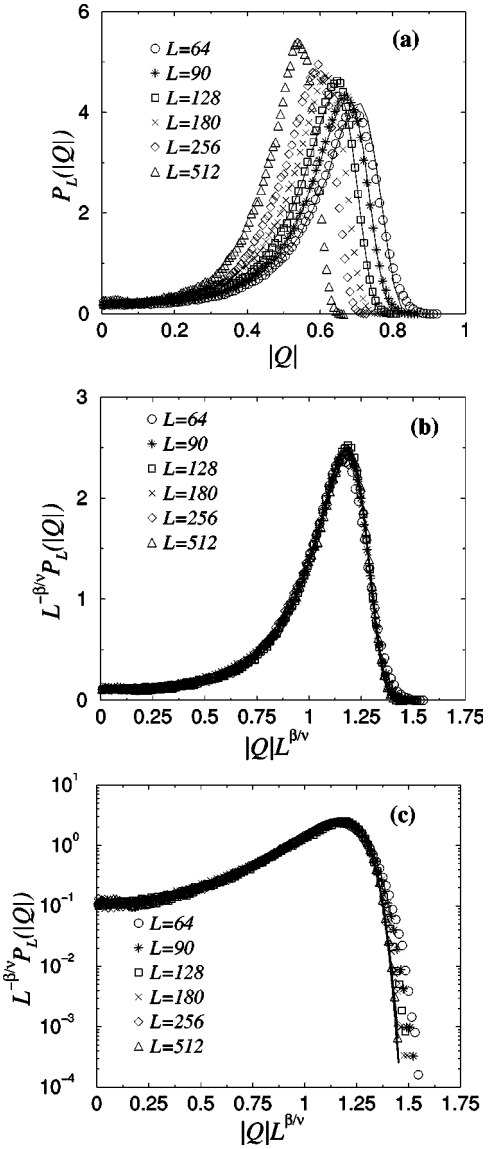

FIG. 13. Order-parameter histograms $P_L(|Q|)$ at $T=0.8T_c$ and $H_0=0.3J$ for various system sizes at Θ_c. The thin solid lines represent two-dimensional *equilibrium* Ising order-parameter histograms at the critical point for $L=64$, 90, and 128 on all three graphs. (a) Order-parameter distributions. (b) Scaled order-parameter distributions, according to Eq. (20), with $\beta/\nu=1/8$. The bold solid line is the corresponding (Monte Carlo) two-dimensional equilibrium Ising distribution without any additional scaling parameters [53]. (c) Same as in (b) on lin-log scales to enhance the view of the corrections to scaling for small systems at large $|Q|$.

To test this expectation, we performed simulations at $T=0.8T_c$ for field amplitudes ranging from $0.3J$ to infinity with system sizes $L=64$, 90, and 128. [$H_0=\infty$ corresponds to the Glauber spin-flip probabilities [Eq. (3)] being equal to 0 (1) depending on whether the spin is parallel (antiparallel)

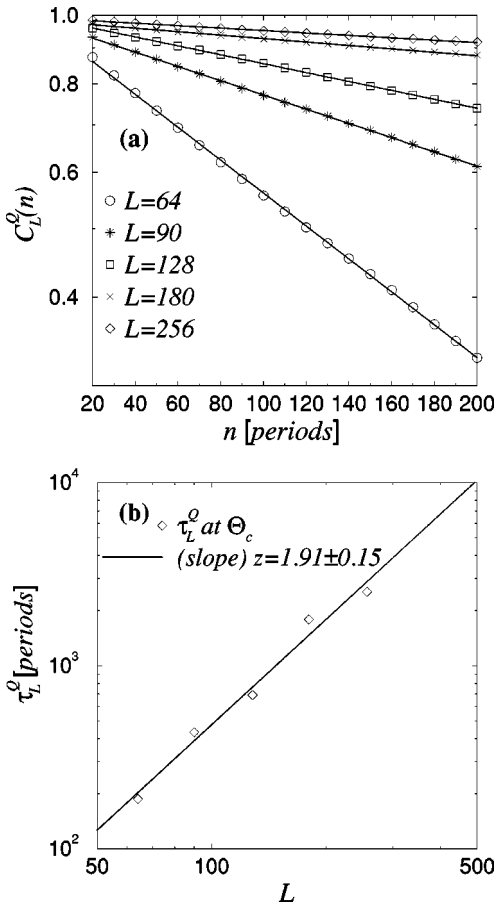

FIG. 14. Critical slowing down for the order parameter at $T=0.8T_c$ and $H_0=0.3J$ at $\Theta=\Theta_c$. (a) The normalized autocorrelation function on a lin-log scale for intermediate times. The straight lines are fits to exponential decays according to Eq. (21). (b) Determining the dynamic exponent, z, using a power-law fit to Eq. (22) (log-log plot).

to the external field, with no influence from the configuration of the neighboring spins.] We further performed runs at $T=0.9T_c$, $T=0.6T_c$, and $T=0.5T_c$ for various field amplitudes with system sizes $L=64$ and 90. The typical run length was 2×10^4 periods. The purpose of these runs was to explore the universal nature of the DPT in the multidroplet regime, and the crossover to the strong-field regime where the DPT should disappear.

In the strong-field regime the droplet picture breaks down, since the individual spins are decoupled. Thus the metastable phase no longer exists, and the decay of the phase having opposite sign to the external field approaches a simple exponential form (which becomes exact in the $H_0\to\infty$ limit). In the Appendix we show that under these conditions the system magnetization always relaxes to a symmetric limit cycle with $Q=0$ for *all* frequencies; thus no DPT can exist.

Figures 15(a), 15(b), and 15(c) show the order parameter vs the dimensionless half-period for $L=64$ and a range of field amplitudes at $T=0.8T_c$, $T=0.6T_c$, and $T=0.5T_c$, respectively. The typical order-parameter profile where the system exhibits the DPT prevails up to some temperature dependent crossover field amplitude $H_\times(T)$ (filled symbols

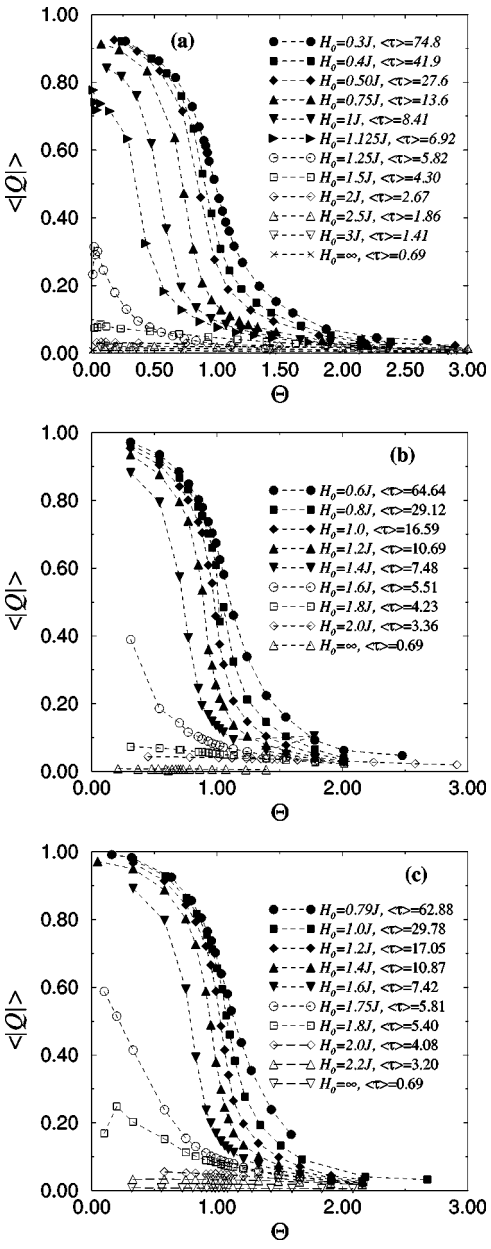

FIG. 15. DPT in the multidroplet regime and strong-field crossover for various temperatures and field amplitudes with $L=64$. Order-parameter profiles with filled symbols exhibit a DPT. Corresponding lifetimes in units of MCSS are also indicated in the figures. (a) $T=0.8T_c$. (b) $T=0.6T_c$. (c) $T=0.5T_c$.

in Fig. 15). For $H_0>H_\times(T)$ the underlying decay mechanism belongs to the strong-field regime, and correspondingly the DPT disappears, as expected.

One can trace this crossover from the multidroplet to the strong-field regime by plotting Θ_c vs H_0/J [Fig. 16(a)] and vs $\langle\tau\rangle$ [Fig. 16(b)] for fixed temperatures. Here again we employed the fourth-order cumulant intersection method using $L=64$ and 90 to identify the infinite-system transition point Θ_c. The crossover to the strong-field regime is indicated by the drop in Θ_c for large fields (small lifetimes).

The DPT in the multidroplet regime $[H_0<H_\times(T)]$ appears to be universal, as can be seen from the scaled order-

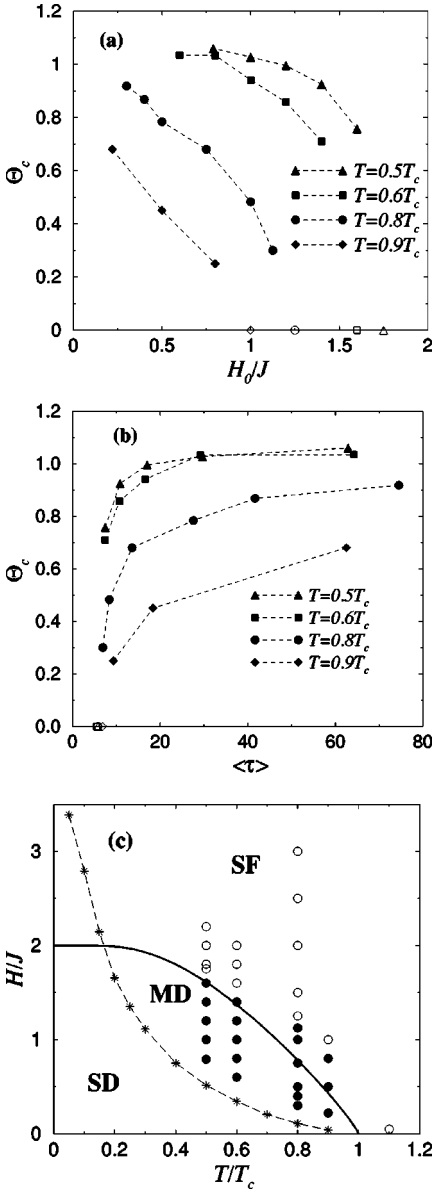

FIG. 16. Scaled critical half-period in the multidroplet-DPT regime (a) as a function of the external field amplitude H_0, and (b) as a function of the lifetime $\langle \tau \rangle$. In (a) the corresponding empty symbols for each temperature on the horizontal axis represent the points which are the MC upper bounds for the crossover field amplitude $H_\times(T)$, beyond which no DPT can be found for any nonzero Θ. In (b) the corresponding empty symbols are the lower bounds for the lifetime below which no DPT is observed. (c) Metastable phase diagram for the kinetic Ising model, based on metastable decay in static fields [15], with the location of our square-wave hysteresis simulations superimposed. The stars connected by a dashed line give a numerical estimate for the dynamic spinodal for our smallest system, $L=64$, that separates the multidroplet (MD) regime from the single-droplet (SD) regime [15]. The solid line is an analytic estimate for the ''mean-field spinodal'' which separates the MD from the strong-field (SF) regime [15]. The circles represent the temperature and field amplitude values at which we ran our simulations. The filled circles indicate points where the system exhibits a DPT, and empty circles represent points where it does not.

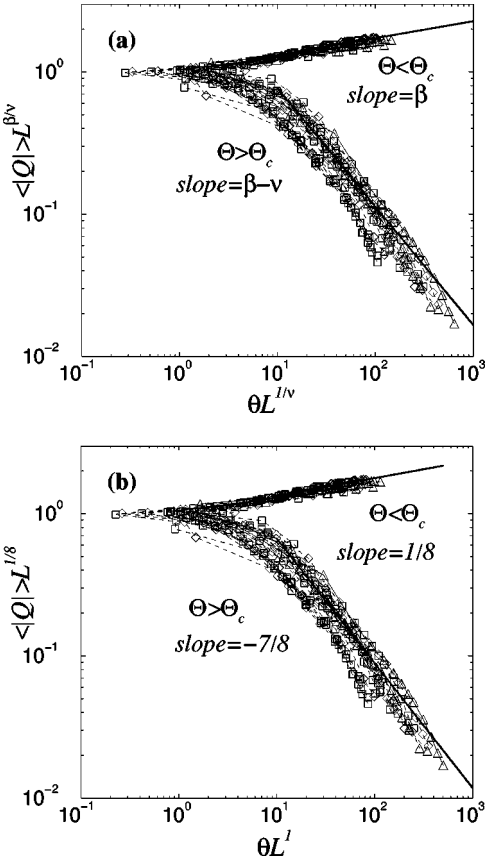

FIG. 17. Universality of the DPT in the multidroplet regime. (a) Finite-size scaling (full data collapse) for the order parameter $\langle |Q| \rangle_L$ (log-log plot). The figure contains 28 DPT data sets: three different temperatures, with four different field amplitudes for each, and at least two different system sizes ($L=64$,90, and 128 at $T=0.8T_c$, and $L=64$ and 90 at $T=0.6T_c$ and $T=0.5T_c$) for all these parameters. The temperature and field values were chosen such that the system is in the multidroplet (MD) regime [filled circles in Fig. 16(c)]. We used $\beta/\nu=1/8$, $\gamma/\nu=7/4$ (two-dimensional equilibrium Ising values), and $\nu=0.95$, the optimal value, as described in Sec. III B. Straight lines represent the asymptotic large-argument behaviors of the scaling functions $\mathcal{F}_\pm$ given by Eq. (12). (b) is the same as (a), except that the exact Ising exponent $\nu=1.0$ is used.

parameter plot in Fig. 17. Note that both graphs contain 28 DPT data sets: three different temperatures, with four different field amplitudes for each, and at least two different system sizes ($L=64$,90, and 128 at $T=0.8T_c$, and $L=64$ and 90 at $T=0.6T_c$ and $T=0.5T_c$) for all these parameters. While the slopes in the asymptotic scaling regime appear to be the same, the small parallel shift may be the result of the nonuniversal critical amplitudes at different temperatures and fields, or simply our inaccuracy in determining $\Theta_c(T,H_0)$, due to the relatively short runs.

On the other hand, as expected, the system shows no singularity, and $\langle |Q| \rangle \overset{L\to\infty}{\to} 0$ for *any* nonzero frequency in the strong-field regime, $H_0 > H_\times(T)$ (see the Appendix). Here the finite-size effects simply reflect the central-limit theorem, i.e., $\langle Q^2 \rangle \sim O(1/L^2)$, or $\langle |Q| \rangle \sim O(1/L)$. Figures 18(a) and 18(b) illustrate this at $T=0.8T_c$, $H_0=1.5J$ and at T

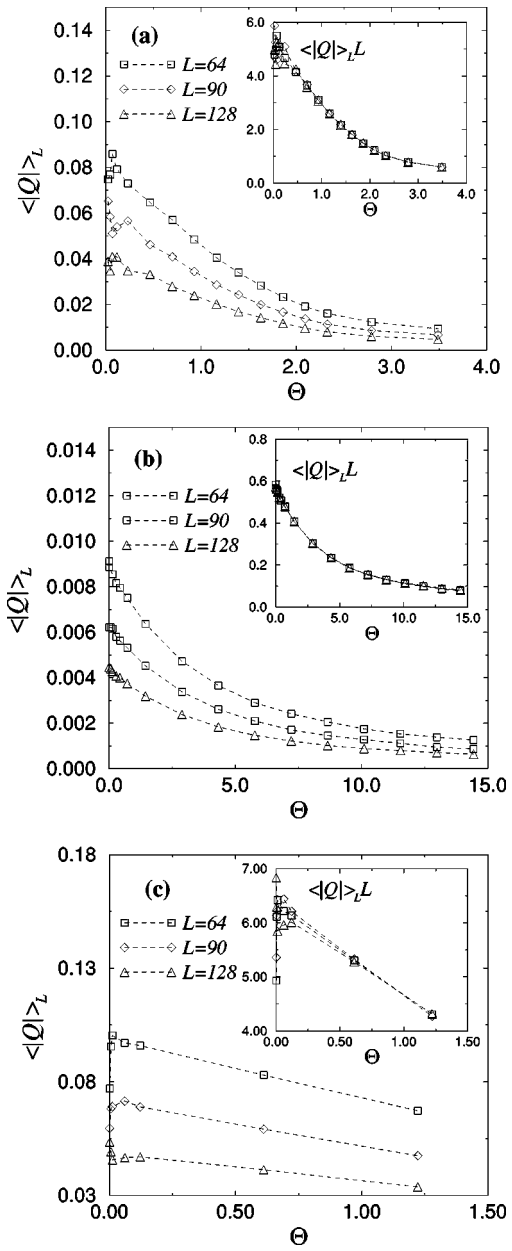

FIG. 18. Order-parameter $\langle|Q|\rangle_L$ behavior outside the multidroplet regime. (a) Strong-field behavior at $T=0.8T_c$ and $H_0=1.5J$ ($\langle\tau\rangle=4.3$ MCSS). (b) Strong-field behavior at $T=0.8T_c$ and $H_0=\infty$ ($\langle\tau\rangle=\ln 2$ MCSS). (c) High-temperature behavior at $T=1.1T_c$ and $H_0=0.05$ ($\langle\tau\rangle=81.8$ MCSS). The insets in all three graphs show data collapse for the scaled order parameter $\langle|Q|\rangle_L L$.

$=0.8T_c$, $H_0=\infty$, respectively. One also expects that a similar behavior prevails at $T>T_c$ for *any* field amplitude, i.e., $H_\times(T)$ vanishes for $T>T_c$. We checked this for $T=1.1T_c$ and $H_0=0.05J$, and the results confirm the $\langle|Q|\rangle\sim O(1/L)$ scaling of the order parameter for all frequencies, showing none of the characteristic finite-size effects of a DPT [Fig. 18(c)]. This result is in distinct disagreement with older work such as Refs. [29,35], which reported observations of the DPT at temperatures considerably above T_c. For smaller system sizes, however, one may observe nontrivial resonance phenomena for temperatures above T_c [55].

Due to the expected complications of a divergent *equilibrium* correlation length, we did not perform simulations at T_c. However, we conjecture that $H_\times(T)$ vanishes at T_c. We expect this conjecture to be extremely difficult to prove or disprove numerically, due to very large and possibly complicated finite-size effects.

IV. CONCLUSIONS AND OUTLOOK

In this paper we have studied the hysteretic response of a spatially extended bistable system exhibiting a DPT. Our model system is the two-dimensional kinetic Ising ferromagnet below its equilibrium critical temperature, subject to a periodic square-wave applied field. The results indicate that for field amplitudes and temperatures such that the metastable phase decays via the multidroplet mechanism, the system undergoes a continuous dynamic phase transition when the half-period of the field, $t_{1/2}$, is comparable to the metastable lifetime, $\langle\tau(T,H_0)\rangle$. Thus the critical value Θ_c of the dimensionless half-period defined in Eq. (7) is of order unity. As Θ is increased beyond Θ_c, the order parameter $\langle|Q|\rangle$ (the expectation value of the norm of the period-averaged magnetization) vanishes [Fig. 5(a)], displaying singular behavior at the critical point, as shown in Figs. 5(b) and 5(c).

The characteristic finite-size effects in the order parameter and its fluctuations indicate that there is a divergent correlation length associated with the transition. We used standard finite-size scaling techniques adopted from the theory of equilibrium phase transitions. We estimated Θ_c and the critical exponents β, γ, and ν from relatively high precision data for system sizes between $L=64$ and 512 at $T=0.8T_c$ and $H_0=0.3J$. Our best estimates are $\beta/\nu=0.126\pm0.005$, $\gamma/\nu=1.74\pm0.05$, and $\nu=0.95\pm0.15$. These values agree within statistical errors with those previously obtained with a sinusoidally oscillating field [27,28], providing strong evidence that the shape of the field oscillation does not affect the universal aspects of the DPT. Observing the stationary autocorrelation function, we also saw that at the transition point the system exhibits critical slowing down governed by the dynamic exponent $z=1.91\pm0.15$. Although the local Glauber dynamic for the spins does not directly predict any specific dynamic for the period-averaged spins, $\{Q_i\}$, we note that this is also very close to the corresponding exponent $z=2.12(5)$, measured in standard two-dimensional Ising simulations with local dynamics [54]. Our best values for the exponent ratios β/ν and γ/ν are given with relatively high confidence, while for ν it is rather poor. In this sense tracking down the exponent ν and obtaining an accurate estimate for it remains elusive. Note, however, that we could only rely on the standard (single spin-flip) MC algorithm, since we had to preserve the underlying dynamics. Using more sophisticated algorithms to avoid the critical slowing down as seen in Figs. 6 and 14, would require an underlying ''Hamiltonian'' for the corresponding *local* order parameter $\{Q_i\}$, which is not yet known. While in a coarse-grained and universal sense a ϕ^4 Hamiltonian is supported by our data, it does not point to any one particular microscopic Hamiltonian for the microscopic order parameter $\{Q_i\}$. However, a ϕ^4 coarse-grained Hamiltonian for $\{Q_i\}$ was recently derived,

starting from the time-dependent Ginzburg-Landau equation for the magnetization [44].

Of the known universality classes, our exponent estimates for the DPT are closest (and within the statistical errors) to those of the the two-dimensional equilibrium Ising model: $\beta/\nu=1/8=0.125$, $\gamma/\nu=7/4=1.75$, and $\nu=1$. Consequently, our measured exponent ratios satisfy the hyperscaling relation

$$2(\beta/\nu)+\gamma/\nu=1.99\pm0.05\approx d, \tag{23}$$

where $d=2$ is the spatial dimension [57]. Further, the fixed-point value of the fourth-order cumulant, $U^*=0.611\pm0.003$, is also extremely close to that of the Ising model, $U^*=0.6106901(5)$ [56]. These findings provide conclusive evidence that the DPT indeed corresponds to a non-trivial fixed point. We tested the full data collapse for the scaled order parameter and its variance, as shown in Fig. 11, and it confirmed the existence of the universal scaling functions given by Eqs. (12) and (13). Also, at the critical frequency, the order-parameter distributions follow finite-size scaling predictions [Eq. (20)], as shown in Fig. 13. More surprisingly, the critical DPT order-parameter distributions coincide with those of the two-dimensional equilibrium Ising model at the critical temperature (except for stronger corrections to scaling), *without* any additional fitting of the underlying microscopic length scale.

While our finite-size scaling data clearly indicate the existence of a divergent length scale, we did not measure the correlation length for the *local* order parameter directly. Future studies may include extracting the correlation length ξ_Q from the $\langle Q_i Q_j\rangle$ correlations (or from the corresponding structure factor). This approach would also provide another way to measure the exponent ν by plotting ξ_Q vs θ in the critical regime for large systems, and assuming $\xi_Q\sim\theta^{-\nu}$.

We also studied the universal aspects of the DPT at other temperatures and fields. Shorter runs at $T=0.8T_c$, $T=0.6T_c$, and $T=0.5T_c$ for field amplitudes $H_0<H_\times(T)$ also confirmed scaling and the universality of the DPT (Fig. 17). The condition for the field amplitude implies that the system only exhibits a DPT in the multidroplet regime. For $H_0>H_\times(T)$ strong-field behavior governs the decay of the magnetization, and the DPT disappears, as indicated by Fig. 16 and Figs. 18(a) and 18(b). We also found that the high-temperature phase is qualitatively similar to the strong-field regime in that there is no sign of a DPT for $T>T_c$ [Fig. 18(c)].

One may ask how general the phenomenon of a DPT is in spatially extended bistable systems, subject to a periodic applied ''field'' which drives the system between its metastable and stable ''wells.'' It is possible that having up-down symmetry of the period-averaged ''magnetization'' is sufficient for possessing a Hamiltonian at the coarse-grained level, even if the system is driven far away from equilibrium and is microscopically irreversible [58]. Future research can address this question by studying other systems (not necessarily ferromagnets) that exhibit hysteresis.

ACKNOWLEDGMENTS

We thank S. W. Sides, S. J. Mitchell, and G. Brown for stimulating discussions. We would like to thank W. Janke for providing us with data from Ref. [53] for comparison of the critical order-parameter distributions. We acknowledge support by the U.S. Department of Energy through the former Supercomputer Computations Research Institute, by the Center for Materials Research and Technology at Florida State University, and by the U.S. National Science Foundation through Grant Nos. DMR-9634873, DMR-9871455, and DMR-9981815. This research also used resources of the National Energy Research Scientific Computing Center, which is supported by the Office of Science of the U.S. Department of Energy under Contract No. DE-AC03-76SF00098.

APPENDIX: LOW-FREQUENCY AND STRONG-FIELD MEAN-FIELD APPROXIMATION

For simplicity, in the following we assume that the magnetization decays from $m=+1$ to $m=-1$ after a *single* field reversal ($H_0\rightarrow -H_0$). This is a good approximation below the equilibrium critical temperature ($m_{\rm sp}\approx 1$), and for any temperature when $H_0\rightarrow\infty$. Further, we assume that the volume fraction of metastable or unstable spins follows a simple monotonic decay, $\hat{\varphi}(t)$.

In terms of the volume fraction of *positive* spins, $\phi(t)$, the magnetization can be written as

$$m(t)=2\phi(t)-1. \tag{A1}$$

Subject to a square-wave field,

$$H(t)=\begin{cases} -H_0 & 0\leqslant t<t_{1/2} \\ +H_0 & t_{1/2}\leqslant t<2t_{1/2}, \end{cases} \tag{A2}$$

in the first (second) half-period the volume fraction of the positive (negative) spins decays according to $\hat{\varphi}(t)$. Thus, in each period (measuring time t from the beginning of the period),

$$\phi(t)\approx\begin{cases} \phi(0)\hat{\varphi}(t), & 0\leqslant t\leqslant t_{1/2} \\ 1-[1-\phi(t_{1/2})]\hat{\varphi}(t-t_{1/2}), & t_{1/2}\leqslant t\leqslant 2t_{1/2}. \end{cases} \tag{A3}$$

Using this approximation, one directly obtains a linear mapping

$$\phi_{n+1}=1-[1-\phi_n\hat{\varphi}(t_{1/2})]\hat{\varphi}(t_{1/2}), \tag{A4}$$

where $\phi_n\equiv\phi(2nt_{1/2})$ is the volume fraction of the positive spins at the beginning of the nth period, $n=0,1,2,\ldots$. The stationary value of this quantity is

$$\phi^*=\lim_{n\rightarrow\infty}\phi_n=\frac{1}{1+\hat{\varphi}(t_{1/2})}. \tag{A5}$$

Consequently, the magnetization reaches a stationary limit cycle

$$m(t)\approx\begin{cases}\dfrac{2}{1+\hat{\varphi}(t_{1/2})}\hat{\varphi}(t)-1 & 0\leqslant t\leqslant t_{1/2}\\[2ex] 1-\dfrac{2}{1+\hat{\varphi}(t_{1/2})}\hat{\varphi}(t-t_{1/2}) & t_{1/2}\leqslant t\leqslant 2t_{1/2}.\end{cases} \tag{A6}$$

In this limit cycle the magnetization oscillates about zero,

$$m(0)=-m(t_{1/2})=\frac{1-\hat{\varphi}(t_{1/2})}{1+\hat{\varphi}(t_{1/2})}, \tag{A7}$$

and the symmetry of the magnetization, $m(t\pm t_{1/2})=-m(t)$, implies

$$Q=\frac{1}{2t_{1/2}}\oint m(t)dt=0. \tag{A8}$$

This corresponds to the symmetric (dynamically disordered) phase. Note that this symmetric phase is always reached when $\hat{\varphi}(t)$ decreases monotonically from unity at $t=0$ to zero as $t\to\infty$.

In the multidroplet regime, the volume fraction of the metastable phase decays according to Avrami's law [17,18]. In the low-frequency limit, $t_{1/2}\gg\langle\tau\rangle$ $(\Theta\gg 1)$, each half-period almost always contains a *complete* metastable decay [Fig. 2(a)]. Avrami's law for the metastable volume fraction in each half-period can then be directly applied using $\hat{\varphi}(t)=\varphi_{\rm ms}(t)\approx e^{-(\ln 2)t^3/\langle\tau\rangle^3}$ [17,18]. This functional form for $\varphi_{\rm ms}(t)$ breaks down when $t_{1/2}$ becomes comparable to $\langle\tau\rangle$ $(\Theta\approx 1)$; thus this simple mean-field approximation cannot predict any instability related to the DPT.

In the $H_0\to\infty$ limit the individual spins become decoupled. Then one can obtain $\hat{\varphi}(t)=e^{-(\ln 2)t/\langle\tau\rangle}$ which is exact for *all* frequencies. Further, this exponential decay is a good approximation everywhere in the strong-field regime; thus no DPT can exist there.

[1] J. A. Ewing, Proc. R. Soc. London **33**, 21 (1881).
[2] E. Warburg, Annalen der Physik und Chemie (Neue Folge) **13**, 141 (1881).
[3] J. A. Ewing, Proc. R. Soc. London **34**, 39 (1882).
[4] C. P. Steinmetz, Trans. Am. Inst. Electr. Eng. **9**, 3 (1892).
[5] A. Aharoni, *Introduction to the Theory of Ferromagnetism* (Clarendon, Oxford, 1996).
[6] H. M. Duiker and P. D. Beale, Phys. Rev. B **41**, 490 (1990); P. D. Beale, Integr. Ferroelectr. **4**, 107 (1994).
[7] M. Rao and R. Pandit, Phys. Rev. B **43**, 3373 (1991).
[8] V. N. Smelyanskiy, M. I. Dykman, H. Rabitz, B. E. Vugmeister, S. L. Bernasek, and A. B. Bocarsly, J. Chem. Phys. **110**, 11 488 (1999).
[9] S. J. Mitchell, G. Brown, and P. A. Rikvold, J. Electroanal. Chem. **493**, 68 (2000); Surf. Sci. (to be published) (e-print, cond-mat/0007079).
[10] A. Cheng and M. Caffrey, J. Phys. Chem. **100**, 5608 (1996).
[11] Y. He and G.-C. Wang, Phys. Rev. Lett. **70**, 2336 (1993).
[12] Q. Jiang, H.-N. Yang, and G.-C. Wang, Phys. Rev. B **52**, 14 911 (1995); J. Appl. Phys. **79**, 5122 (1996).
[13] J. H. Suen and J. L. Erskine, Phys. Rev. Lett. **78**, 3567 (1997); J. H. Suen, M. H. Lee, G. Teeter, and J. L. Erskine, Phys. Rev. B **59**, 4249 (1999).
[14] P. A. Rikvold, M. A. Novotny, M. Kolesik, and H. L. Richards, in *Dynamical Properties of Unconventional Magnetic Systems*, edited by A. T. Skjeltorp and D. Sherrington (Kluwer, Dordrecht, 1998) p. 307; M. Kolesik, M. A. Novotny, and P. A. Rikvold, Phys. Rev. B **56**, 11 791 (1997).
[15] P. A. Rikvold, H. Tomita, S. Miyashita, and S. W. Sides, Phys. Rev. E **49**, 5080 (1994); H. L. Richards, S. W. Sides, M. A. Novotny, and P. A. Rikvold, J. Magn. Magn. Mater. **150**, 37 (1995); P. A. Rikvold and B. M. Gorman, in *Annual Reviews of Computational Physics I*, edited by D. Stauffer (World Scientific, Singapore, 1994), p. 149.
[16] H. Tomita and S. Miyashita, Phys. Rev. B **46**, 8886 (1992).
[17] A. N. Kolmogorov, Bull. Acad. Sci. USSR, Phys. Ser. **1**, 355 (1937); W. A. Johnson and R. F. Mehl, Trans. Am. Inst. Min., Metall. Eng. **135**, 416 (1939); M. Avrami, J. Chem. Phys. **7**, 1103 (1939); **8**, 212 (1940); **9**, 177 (1941).
[18] R. A. Ramos, P. A. Rikvold, and M. A. Novotny, Phys. Rev. B **59**, 9053 (1999).
[19] P. Jung, G. Gray, R. Roy, and P. Mandel, Phys. Rev. Lett. **65**, 1873 (1990).
[20] M. Rao, H. R. Krishnamurthy, and R. Pandit, Phys. Rev. B **42**, 856 (1990).
[21] T. Tomé and M. J. de Oliveira, Phys. Rev. A **41**, 4251 (1990).
[22] J. F. F. Mendes and J. S. Lage, J. Stat. Phys. **64**, 653 (1991).
[23] M. F. Zimmer, Phys. Rev. E **47**, 3950 (1993).
[24] W. S. Lo and R. A. Pelcovits, Phys. Rev. A **42**, 7471 (1990).
[25] S. W. Sides, P. A. Rikvold, and M. A. Novotny, J. Appl. Phys. **83**, 6494 (1998).
[26] S. W. Sides, P. A. Rikvold, and M. A. Novotny, Phys. Rev. E **57**, 6512 (1998).
[27] S. W. Sides, P. A. Rikvold, and M. A. Novotny, Phys. Rev. E **59**, 2710 (1999).
[28] S. W. Sides, P. A. Rikvold, and M. A. Novotny, Phys. Rev. Lett. **81**, 834 (1998).
[29] M. Acharyya and B. Chakrabarti, Phys. Rev. B **52**, 6550 (1995).
[30] M. Acharyya, Phys. Rev. E **56**, 1234 (1997).
[31] M. Acharyya, Phys. Rev. E **56**, 2407 (1997).
[32] M. Acharyya, Phys. Rev. E **58**, 179 (1998).
[33] G. M. Buendía and E. Machado, Phys. Rev. B **61**, 14 686 (2000).
[34] G. M. Buendía and E. Machado, Phys. Rev. E **58**, 1260 (1998).
[35] M. Acharyya and B. K. Chakrabarti in *Annual Reviews of Computational Physics I*, edited by D. Stauffer (World Scientific, Singapore, 1994) p. 107.
[36] B. Chakrabarti and M. Acharyya, Rev. Mod. Phys. **71**, 847 (1999).
[37] P. A. Rikvold, G. Korniss, C. J. White, M. A. Novotny, and S. W. Sides, in *Computer Simulation Studies in Condensed Mat-*

ter Physics XII, edited by D. P. Landau, S. P. Lewis, and H.-B. Schüttler, Springer Proceedings in Physics Vol. 85 (Springer, Berlin, 2000), p. 105.

[38] M. E. Fisher and M. N. Barber, Phys. Rev. Lett. **28**, 1516 (1972).

[39] K. Binder and D. W. Heermann, *Monte Carlo Simulation in Statistical Physics. An Introduction*, 3rd ed. (Springer, Berlin, 1997).

[40] K. Binder in *Finite-Size Scaling and Numerical Simulation of Statistical Systems*, edited by V. Privman (World Scientific, Singapore, 1990) p. 173.

[41] D. P. Landau, Phys. Rev. B **13**, 2997 (1976); and in *Finite-Size Scaling and Numerical Simulation of Statistical Systems* (Ref. [40]), p. 225.

[42] B. Schmittmann and R. K. P. Zia, in *Phase Transitions and Critical Phenomena*, edited by C. Domb and J. L. Lebowitz (Academic Press, New York, 1995), Vol. 17.

[43] J. Marro and R. Dickman, *Nonequilibrium Phase Transitions in Lattice Models* (Cambridge University Press, Cambridge, 1999).

[44] H. Fujisaka, H. Tutu, and P. A. Rikvold, Phys. Rev. E (to be published) (e-print cond-mat/0009284).

[45] L. Onsager, Phys. Rev. **65**, 117 (1944).

[46] B. D. Lubachevsky, Complex Syst. **1**, 1099 (1987); J. Comput. Phys. **75**, 103 (1988).

[47] G. Korniss, M. A. Novotny, and P. A. Rikvold, J. Comput. Phys. **153**, 488 (1999).

[48] G. Korniss, Z. Toroczkai, M. A. Novotny, and P. A. Rikvold, Phys. Rev. Lett. **84**, 1351 (2000).

[49] G. Korniss, M. A. Novotny, Z. Toroczkai, and P. A. Rikvold, in *Computer Simulation Studies in Condensed Matter Physics XIII*, edited by D. P. Landau, S. P. Lewis, and H.-B. Schüttler, Springer Proceedings in Physics Vol. 86 (Springer, Berlin, 2001), p. 183.

[50] G. Korniss, P. A. Rikvold, and M. A. Novotny (unpublished).

[51] N. Goldenfeld, *Lectures on Phase Transitions and the Renormalization Group* (Addison-Wesley, Reading, MA, 1992).

[52] The difference between the order-parameter time series in Fig. 3 (strongly fluctuating trace) and Fig. 12(a) is due to the fact that the latter is taken at the infinite-system transition point ($\Theta=\Theta_c=0.918$), while the former is taken at the corresponding finite-system ''critical point'' [$\Theta=\Theta_c(L)=0.98$] where the fluctuations are largest.

[53] O. Dillmann, M. Muller, W. Janke, and K. Binder, in *Computer Simulation Studies in Condensed Matter Physics XII*, edited by D. P. Landau, S. P. Lewis, and H.-B. Schüttler, Springer Proceedings in Physics Vol. 85 (Springer, Berlin, 2000), p. 124.

[54] W. Janke, in *Computational Physics: Selected Methods, Simple Exercises, Serious Applications*, edited by K. H. Hoffmann and M. Schreiber (Springer, Berlin, 1996), p. 10.

[55] K.-t. Leung and Z. Néda, Phys. Lett. A **246**, 505 (1998); Phys. Rev. E **59**, 2730 (1999).

[56] G. Kamieniarz and H. Blöte, J. Phys. A **26**, 201 (1993).

[57] See a further discussion of this point in Ref. [27].

[58] G. Grinstein, C. Jayaprakash, and Y. He, Phys. Rev. Lett. **55**, 2527 (1985).